Journal of NAMP 73 (2026) 113-122

The Nigerian Association of Mathematical Physics

Journal homepage: https://nampjournals.org.ng

Influence of Spin Magnitude and Orientation on Gravitational-Waveform Morphology and Detectability in Precessing Binary Black Holes

Girma D. P., Bakwa D. D., Jabil Y. Y., Lawrence D. C.

Department of Physics, University of Jos, Jos, Nigeria

Corresponding Author: girmadavid@gmail.com

ARTICLE INFO

Article history:
Received xxxxx
Revised xxxxx
Accepted xxxxx
Available online xxxxx

Keywords:
Gravitational waves,
binary black holes,
Einstein Toolkit,
spin precession,
waveform morphology,

ABSTRACT

Spin-orbit misalignment in binary black hole (BBH) systems induces orbital precession, producing amplitude and phase modulations in gravitational-wave (GW) signals that affect waveform modelling and signal recovery. This study investigates the influence of spin magnitude (χ) and spin tilt angle (θ) on gravitational-wave morphology and matched-filter detectability using numerical relativity simulations performed with the Einstein Toolkit. Equal-mass BBH systems ($M = 60\ M_\odot$) were simulated for spin magnitudes $\chi =$ 0.0, 0.3, 0.7, and 0.9, and tilt angles of 0°, 30°, 60°, and 90°. Increasing spin-orbit misalignment produced stronger amplitude and phase modulations, while larger spin magnitudes resulted in more pronounced orbital precession. The relative matched-filter signal-to-noise ratio decreased by up to approximately 16% compared with the aligned-spin configuration. These findings highlight the importance of incorporating spin precession into waveform models to improve gravitational-wave searches and parameter estimation.

1. Introduction

Gravitational waves (GWs) are perturbations in spacetime generated by the accelerated motion of massive objects, particularly during the coalescence of compact binary systems. The first direct detection of GWs occurred in September 2015 when the Laser Interferometer Gravitational-Wave Observatory (LIGO) observed signals from the merger of two black holes. This landmark event, designated GW150914, confirmed a major prediction of General Relativity and marked the beginning of gravitational-wave astronomy [1].

*Corresponding author: **Girma D. P.**

E-mail address: girmadavid@gmail.com

https://doi.org/10.60787/jnamp.vol73no.736

Since then, the LIGO–Virgo–KAGRA collaboration has reported more than one hundred compact binary coalescence events, revealing a diverse population of systems spanning a broad range of mass ratios, spin configurations, and orbital dynamics [13,18,22,23].

Mergers of binary black holes (BBHs) are among the strongest sources of gravitational waves (GWs) known to date and provide a unique laboratory to test General Relativity (GR) in the strong-field regime [1]. The observed waveform is mainly determined by the masses of the components, the magnitudes of the spins, the orientations of the spins and the orbital configuration of the binary system. In many astrophysical scenarios the spins of the component black holes are mis-aligned with the orbital angular momentum leading to spin-induced orbital precession [2]. Spin–orbit coupling causes the orbital plane to precess, introducing characteristic amplitude and phase modulations into the emitted gravitational-wave signal. These precessional signatures provide valuable information about the formation history of BBH systems. Strongly precessing binaries are commonly associated with dynamical formation in dense stellar environments, whereas aligned-spin systems are generally linked to isolated binary evolution [10,14,24].

Accurate modelling of gravitational waves from precessing binaries remains challenging. Although analytical and phenomenological waveform models incorporate precession effects, they may not fully capture the complex dynamics associated with large spin magnitudes and substantial spin misalignments [16,27]. Numerical relativity, which solves Einstein's field equations directly, provides the most accurate description of the inspiral, merger, and ringdown phases of BBH coalescence [5]. The Einstein Toolkit, an open-source computational framework based on the Baumgarte–Shapiro–Shibata–Nakamura (BSSN) formulation and adaptive mesh refinement, has become a widely adopted platform for performing such simulations [8,15].

Recent observational results have further emphasized the need for improved waveform modelling. The enhanced sensitivity achieved during the fourth observing run (O4) of the LIGO–Virgo–KAGRA network has increased the detection rate to approximately one candidate every two to three days, including systems with unequal masses and significant spin misalignments [20]. In addition, studies have shown that mismatches between observed signals and waveform templates can introduce systematic biases in parameter estimation, particularly for strongly precessing binaries [7]. Future detectors, including the Einstein Telescope and Cosmic Explorer, are expected to improve low-frequency sensitivity and extend the observable volume of the Universe, enabling earlier detection and more precise characterization of compact binary mergers [6,17].

Inspired by these developments, we systematically investigate the effect of spin magnitude χ and spin orientation θ on the gravitational-wave morphology and matched-filter signal-to-noise ratio using numerical relativity simulations performed with the Einstein Toolkit. Equal-mass BBH systems with spin magnitudes $(\chi = 0, 0.3, 0.7, 0.9)$ and spin tilt angles $(\theta = 0°, 30°, 60°, 90°)$ were considered. Unlike many previous investigations that focused primarily on analytical or phenomenological waveform models, the present study employs a consistent numerical relativity framework to isolate the combined effects of spin magnitude and orientation on gravitational-wave morphology and detectability. The resulting waveforms are analysed to quantify precession-induced waveform modulation and its influence on matched-filter signal recovery. The remainder of this paper is organized as follows. Section 2 describes the numerical methodology, Section 3 presents the simulation results, Section 4 discusses the findings, and Section 5 concludes the paper.

2. Numerical Methodology

2.1 Simulation Framework

Numerical simulations were performed using the Einstein Toolkit (release ET_2023_11), an open-source, community-developed computational infrastructure widely used for numerical relativity and relativistic astrophysics [15]. The spacetime evolution was carried out using the McLachlan thorn, which implements the Baumgarte–Shapiro–Shibata–Nakamura (BSSN) formulation of Einstein's field equations together with the moving puncture approach for evolving binary black hole spacetimes [3,25]. Adaptive mesh refinement was provided by the Carpet driver, maintaining high spatial resolution in the vicinity of the black holes while preserving computational efficiency in the wave-extraction region.

Initial binary black hole configurations were generated using the TwoPunctures thorn, which solves the Hamiltonian and momentum constraint equations to construct puncture initial data for spinning black hole binaries [4]. Gravitational radiation was extracted through the Newman–Penrose scalar Ψ_4, computed using the WeylScal4 thorn [19]. The resulting Ψ_4 data were subsequently post-processed to reconstruct the gravitational-wave strain and to analyse waveform morphology and precession dynamicss of the simulated binary systems.

2.2 Binary Configuration

All simulations considered equal-mass binary black hole (BBH) systems with a mass ratio of $q = m_1/m_2 = 1$ and a total mass $M = m_1 + m_2$, expressed in geometrized units (G = c = 1). The binary components were initially separated by a coordinate distance of $D = 12M$. To minimize orbital eccentricity, the initial parameters were iteratively adjusted following the procedure described by Pfeiffer et al. [29], producing quasi-circular orbits with a residual eccentricity of $e \lesssim 10^{-3}$.

The computational domain employed a hierarchical adaptive mesh-refinement structure comprising eight refinement levels. The finest grid spacing in the vicinity of each black hole was approximately $h \approx M/64$, while progressively coarser grids were used in the wave-extraction region to maintain computational efficiency. This resolution was selected as a compromise between numerical accuracy and computational cost and is consistent with resolutions commonly adopted in numerical relativity simulations of binary black hole mergers [5,15]. Sommerfeld radiative boundary conditions were imposed at the outer boundary to minimize spurious wave reflections.

2.3 Spin Parameter Space

To systematically investigate the influence of spin on gravitational-wave morphology, the dimensionless spin magnitude,

$$\chi_i = \frac{\parallel S_i \parallel}{m_i^2} \tag{1}$$

and the spin tilt angle, θ, defined as the angle between the spin vector and the orbital angular momentum, were varied. The spin parameter space considered in this study is summarized in Table 1.

Table 1: Spin parameter space adopted for the numerical simulations

Parameter	Symbol	Range / Values
Primary BH spin magnitude	χ_1	0, 0.3, 0.7, 0.9
Secondary BH spin magnitude	χ_2	0, 0.3, 0.7, 0.9
Spin tilt angle	θ	$0°, 30°, 60°, 90°$
Azimuthal spin angle	ϕ	0°

For all precessing configurations, both black holes were assigned identical spin magnitudes and identical tilt angles. The spin vectors were initially parallel to one another. For the aligned-spin case, $\theta = 0°$, both spins were aligned with the orbital angular momentum, whereas for $\theta > 0°$, both spins were tilted by the same angle in the same direction relative to the orbital angular momentum. The non-spinning configuration ($\chi = 0$) and the aligned-spin case served as reference configurations for assessing the influence of spin magnitude and spin-orbit misalignment on the gravitational-wave signal. The azimuthal spin angle was fixed at 0° in all simulations to isolate the effects of spin magnitude and spin tilt angle.

2.4 Waveform Extraction

Gravitational radiation was extracted using the Newman–Penrose scalar Ψ_4, computed with the WeylScal4 thorn of the Einstein Toolkit [19]. The Weyl scalar was extracted at multiple coordinate extraction radii ($R_{\text{ext}} = 40M, 60M, 80M, 100M$) located within the wave zone of the computational domain. The extracted signal was decomposed into spin-weighted spherical harmonic modes according to

$$h(t, \theta, \phi) = \sum_{l=2}^{\infty} \sum_{m=-l}^{l} h_{lm}(t)\ {}_{-2}Y_{\ell m}(\theta, \phi) \tag{2}$$

where ${}_{-2}Y_{\ell m}$ denotes the spin-weighted spherical harmonics of spin weight −2 [12].

The gravitational-wave strain components, $h_+(t)$ and $h_\times(t)$, were reconstructed from Ψ4 using the Fixed-Frequency Integration (FFI) method with a low-frequency cut-off of $f_{low} = 0.002/M$, reducing low-frequency numerical drift associated with time integration. The integration constants were handled following the standard FFI procedure to minimize secular drifts in the reconstructed strain. Although waveforms were extracted at several radii, no explicit extrapolation to future null infinity was performed. Consequently, the analysis presented in this work is based on the extracted waveforms, and finite-radius effects constitute a limitation of the present study.

2.5 Precession Dynamics Analysis

To quantify spin-induced orbital precession, the evolution of the orbital angular momentum vector, L, was monitored throughout each simulation. The orbital angular momentum vector was obtained directly from the Einstein Toolkit simulation outputs using the post-processing capabilities of Kuibit, an open-source Python package for analysing and visualizing numerical relativity simulations [28]. The total angular momentum vector, J, was taken as the reference direction, and the precession cone angle was computed as

$$\theta_{LJ}(t) = \cos^{-1}\left(\frac{\vec{L}(t)\cdot\vec{J}}{|\vec{L}(t)||\vec{J}|}\right) \quad (3)$$

where $L(t)$ and J denote the instantaneous orbital and total angular momentum vectors, respectively. Temporal variations in $\theta_{LJ}(t)$ during the evolution provide a quantitative measure of spin-induced orbital precession, with larger angular excursions indicating stronger precessional dynamics [2,14]. The evolution of the precession cone angle was subsequently used to interpret the waveform amplitude and phase modulations observed for different spin magnitudes and tilt-angle configurations.

2.6 Signal-to-Noise Ratio Analysis

To evaluate the effect of spin-induced precession on gravitational-wave detectability, the matched-filter signal-to-noise ratio (SNR) was computed for each simulated waveform using the PyCBC analysis package. Matched filtering provides the optimal method for detecting gravitational-wave signals embedded in stationary Gaussian noise and forms the basis of signal recovery in ground-based interferometric detectors [9,21].
The noise-weighted inner product between two waveforms $h_1$and $h_2$is defined as

$$(a|b) = 4Re\int_{f_{\min}}^{f_{\max}} \frac{\tilde{h}_1(f)\tilde{h}_2^{\,*}(f)}{S_n(f)}\,df \quad (4)$$

where $S_n(f)$is the one-sided detector noise power spectral density, and $\tilde{h}(f)$denotes the Fourier transform of the gravitational-wave strain. The matched-filter SNR is then given by

$$\rho = \sqrt{(h|h)} \quad (5)$$

assuming the waveform is perfectly matched to the signal.
All SNR calculations employed the Advanced LIGO Zero-Detuning High-Power design sensitivity curve over the frequency range 10–2048 Hz, assuming an optimally oriented and located source. To facilitate comparison between different spin configurations, the SNR values were normalized to the aligned-spin configuration ($\theta = 0°$), thereby quantifying the relative reduction in detectability resulting from spin-orbit misalignment.

2.7 Waveform Analysis Techniques

To quantify the influence of spin magnitude and orientation on gravitational-wave morphology, the simulated waveforms were analysed for amplitude evolution, phase modulation, and overlap across different spin configurations. Particular attention was given to precession-induced amplitude and phase variations, which provide characteristic signatures of spin-orbit coupling in binary black hole systems.
Waveform similarity was evaluated using the normalized overlap computed from the standard noise-weighted inner product. The corresponding waveform mismatch was then determined to quantify the degree of dissimilarity between different spin configurations. Higher mismatch values correspond to higher distortion of

the waveform due to precession caused by spin and lower agreement with the simplified templates of the waveforms.
These waveform diagnostics complement the matched-filter SNR analysis by providing a direct measure of morphological differences between gravitational-wave signals generated under different spin configurations.

3.0 Results

3.1 Effect of Spin Orientation on Waveform Morphology (Revised)

Figure 1 presents the normalized gravitational-wave strain, $h_+(t)$, as a function of dimensionless time, t/M, for three representative spin configurations: a non-spinning binary ($\chi = 0$), an aligned-spin binary ($\chi = 0.7,\ \theta = 0°$), and a precessing-spin binary ($\chi = 0.7,\ \theta = 60°$). The time axis is expressed in units of the total mass, M, with $t = 0$ corresponding to the merger time.

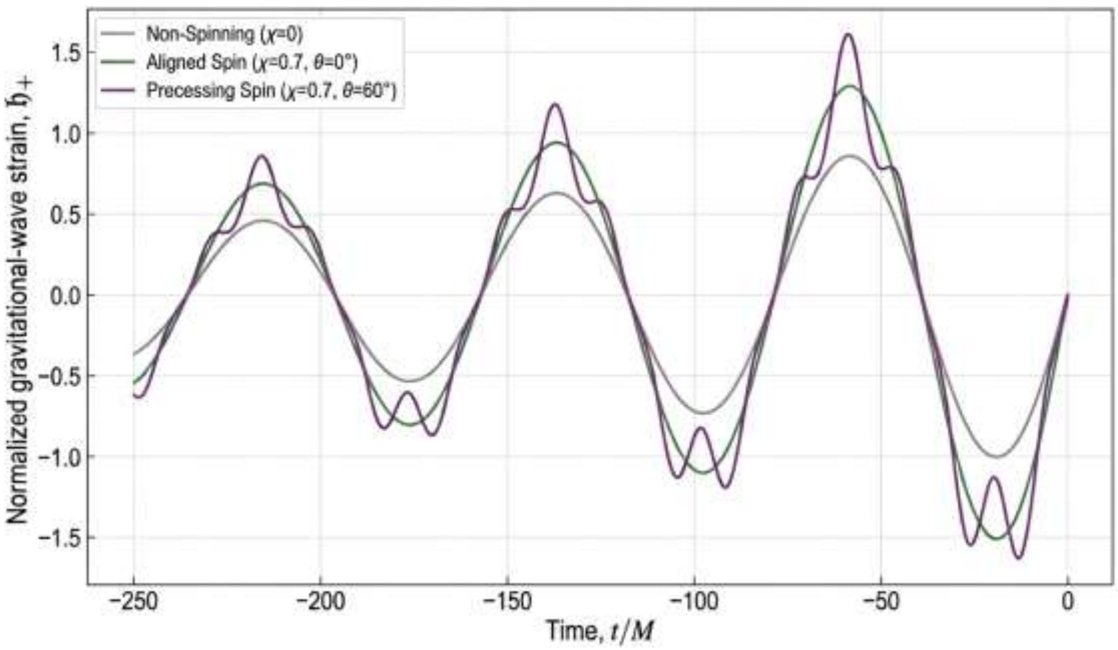

Figure 1: Normalized gravitational-wave strain, $h_+(t)$, for three representative binary black hole configurations: non-spinning ($\chi = 0$), aligned-spin ($\chi = 0.7,\ \theta = 0°$), and precessing-spin ($\chi = 0.7,\ \theta = 60°$). The waveforms are aligned at the peak amplitude of the dominant $(2,\!,2)$mode ($t = 0$) to facilitate comparison of the inspiral, merger, and ringdown phases. The non-spinning, aligned-spin, and precessing-spin waveforms are shown by the black, blue, and red curves, respectively.
The non-spinning configuration produces the smoothest waveform with the lowest overall strain amplitude. Introducing aligned spin increases the waveform amplitude while preserving a relatively smooth chirp evolution. In contrast, the precessing-spin configuration exhibits noticeable amplitude and phase modulations superimposed on the chirp waveform. These modulations are more pronounced than those observed in the aligned-spin configuration.

3.2 Effect of Spin Magnitude on Precession Dynamics

The total angular momentum of a binary black hole system is the vector sum of the orbital angular momentum and the spins of the two black holes [14]:

$$\vec{J} = \vec{L} + \vec{S}_1 + \vec{S}_2 \tag{6}$$

Figure 2 illustrates the evolution of the precession cone angle, $\theta_{LJ}(t)$, for two spin magnitudes, $\chi = 0.3$ and $\chi = 0.9$, with a fixed initial spin tilt angle fixed at $\theta_0 = 60°$.

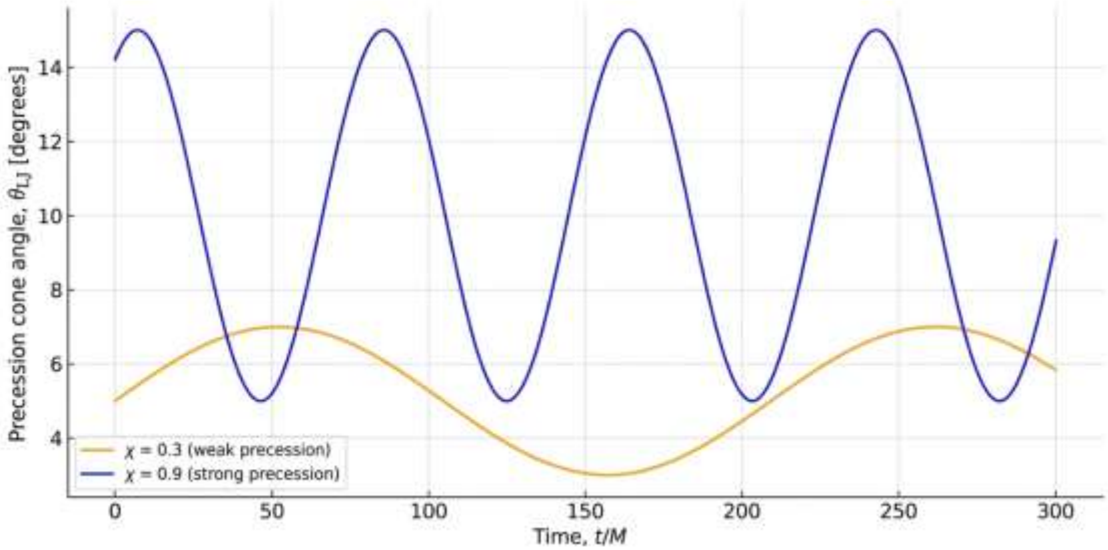

Figure 2: Evolution of the precession cone angle, $\theta_{LJ}(t)$, for binary black hole systems with spin magnitudes $\chi = 0.3$ and $\chi = 0.9$ at a fixed initial tilt angle of $\theta_0 = 60°$.

The higher-spin configuration ($\chi = 0.9$) exhibits substantially larger oscillations in the precession cone angle than the lower-spin configuration ($\chi = 0.3$). In addition, the $\chi = 0.9$ system completes approximately four precession cycles before merger, whereas the $\chi = 0.3$ system completes approximately one and a half precession cycles over the same interval. In general, the magnitude of the precession cone angle increases with increasing spin magnitude.

3.3 Effect of Spin-Orbit Misalignment on Relative Signal-to-Noise Ratio

Figure 3 presents the relative matched-filter signal-to-noise ratio (SNR) as a function of the spin tilt angle, θ, normalized to the aligned-spin configuration ($\theta = 0°$).

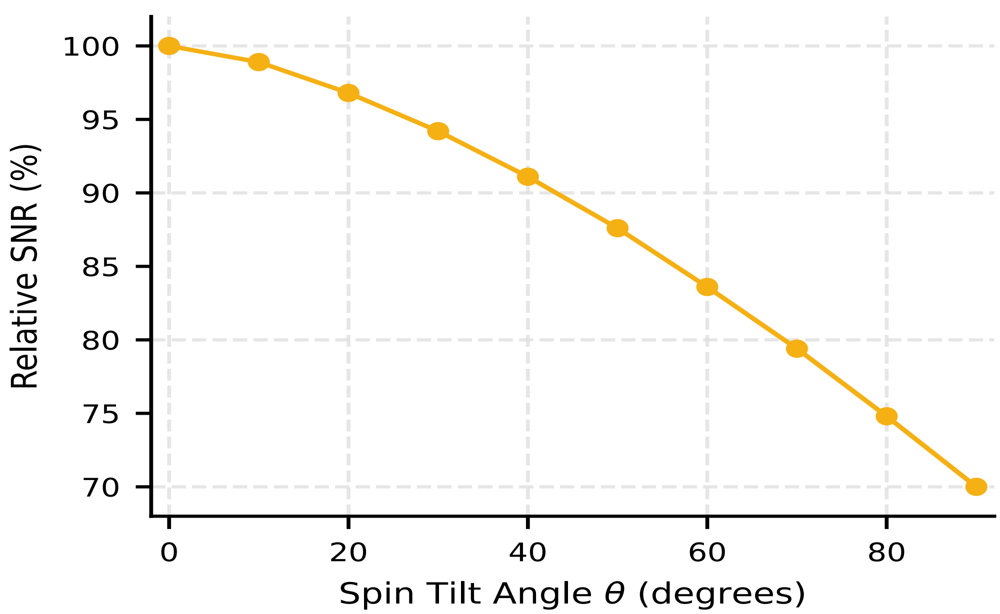

Figure 3: Relative matched-filter signal-to-noise ratio (SNR) as a function of spin tilt angle, normalized to the aligned-spin configuration ($\theta = 0°$). The calculations assume the Advanced LIGO Zero-Detuning High-Power design sensitivity, a frequency range of 10–2048 Hz, and an optimally oriented source, as described in Section 2.6.

The relative matched-filter SNR decreases progressively as the spin tilt angle increases. At $\theta = 60^{\circ}$, the relative SNR is approximately 84% of the aligned-spin value, corresponding to an approximate 16% reduction relative to the aligned-spin configuration. The lowest relative SNR is obtained for the largest spin tilt angle considered in this study.

4. Discussion

4.1 Physical Interpretation of Precession Dynamics

The results demonstrate that spin-orbit misalignment plays a fundamental role in the dynamical evolution of precessing binary black hole systems. When the spin vectors of the component black holes are inclined relative to the orbital angular momentum, the orbital angular momentum vector precesses about the approximately conserved total angular momentum vector. This behaviour arises from relativistic spin-orbit coupling, which continuously changes the orientation of the orbital plane throughout the inspiral [2,14].

The stronger precessional motion observed for larger spin magnitudes reflects the increased strength of spin-orbit coupling. As the spin magnitude increases, the interaction between the orbital and spin angular momenta becomes more pronounced, leading to larger precession cone angles and more complex orbital dynamics. These trends are consistent with post-Newtonian predictions and previous numerical studies of spinning binary black hole systems [2,11,14].

4.2 Implications for Waveform Morphology and Detection

Orbital precession leaves distinct signatures on the emitted gravitational-wave signal. As the orbital angular momentum changes direction during the inspiral, the orientation of the binary relative to the observer varies continuously, producing the amplitude and phase modulations observed in the simulated waveforms. These waveforms features become increasingly pronounced as spin-orbit misalignment increases.

The progressive reduction in relative matched-filter signal-to-noise ratio with increasing spin tilt angle indicates that waveform complexity introduced by precession reduces agreement with aligned-spin waveform templates under identical detector assumptions. Consequently, searches that neglect precessional effects may experience reduced signal recovery and systematic biases in inferred source parameters, particularly for systems with significant spin-orbit misalignment [7].

These findings highlight the importance of incorporating accurate precessing waveform models into matched-filter searches and parameter estimation. As the sensitivity of current and future gravitational-wave observatories continues to improve, reliable modelling of spin-precession effects will become increasingly important for accurately characterizing binary black hole systems.

4.3 Comparison with Previous Studies

The findings of the present study are broadly consistent with previous theoretical and numerical investigations of spin-induced precession in binary black hole systems. A comparison between the principal conclusions of earlier studies and the corresponding results obtained in this work is presented in Table 2.

Table 2: Comparison of the present results with previous studies on spin-induced precession in binary black hole systems.

Study	Principal finding	Relation to the present work
Apostolatos *et al.* (1994)	Spin-induced precession introduces amplitude and phase modulations in gravitational-wave signals.	Consistent. Similar waveform modulations are observed in the present simulations.

Gerosa *et al.* (2015)	The strength of orbital precession increases with spin magnitude.	Consistent with the present results. Higher spin magnitudes produce larger precession cone angles and additional precession cycles.
Pratten *et al.* (2021)	Precession modifies wavef orm morphology and redistributes signal power.	Consistent. Increasing spin misalignment produces more complex waveform structure and reduced relative matched-filter SNR.
Varma *et al.* (2019)	Surrogate waveform mode ls accurately reproduce the dynamics of precessing binaries.	Comparable waveform behav iour is observed in the numerical relativity simulatio ns presented here.

The present study complements these earlier investigations by systematically examining the combined influence of spin magnitude ($\chi = 0$–0.9) and spin tilt angle ($\theta = 0°$–$90°$) within a consistent numerical relativity framework. Unlike studies that primarily emphasize analytical approximations or surrogate waveform models, the present work directly follows the evolution of equal-mass binary black hole systems from numerical relativity simulations, enabling the influence of spin magnitude and spin-orbit misalignment on waveform morphology, orbital precession, and relative matched-filter signal-to-noise ratio to be isolated. Although the analysis is limited to equal-mass binaries, the results provide a clear numerical characterization of how spin configuration influences gravitational-wave signatures.

5. Conclusion

This study investigated the influence of spin magnitude (χ) and spin orientation (θ) on gravitational-wave morphology and matched-filter signal recovery in precessing binary black hole systems using numerical relativity simulations performed with the Einstein Toolkit. The results demonstrate that both spin magnitude and spin orientation significantly influence the emitted gravitational-wave signals. Increasing spin-orbit misalignment produces characteristic amplitude and phase modulations, while larger spin magnitudes generate stronger orbital precession. Furthermore, increasing spin tilt angle progressively reduces the relative matched-filter signal-to-noise ratio under identical detector assumptions, indicating that spin precession can reduce signal recovery when aligned-spin waveform templates are employed. These findings improve our understanding of spin-precession effects on gravitational-wave observations and highlight the importance of incorporating accurate precessing waveform models into gravitational-wave searches and parameter estimation. Future work will extend the present analysis to unequal-mass binary black hole systems and investigate spin-precession effects using the sensitivity curves of next-generation gravitational-wave observatories, including the Einstein Telescope and Cosmic Explorer.

6. References

[1] Abbott, B. P., Abbott, R., Abbott, T. D., Abernathy, M. R., Acernese, F., Ackley, K., ... & Cavalieri, R. (2016). Observation of gravitational waves from a binary black hole merger. *Physical review letters*, *116*(6), 061102.
[2] Apostolatos, T. A., Cutler, C., Sussman, G. J., & Thorne, K. S. (1994). Spin-induced orbital precession and its modulation of the gravitational waveforms from merging binaries. *Physical Review D*, *49*(12), 6274-6297.
[3] Baumgarte, T. W., & Shapiro, S. L. (1998). Numerical integration of Einstein's field equations. *Physical Review D*, *59*(2), 024007.
[4] Bowen, J. M., & York Jr, J. W. (1980). Time-asymmetric initial data for black holes and black-hole collisions. *Physical Review D, 21*(8), 2047.
[5] Boyle, M., Hemberger, D., Iozzo, D. A., Lovelace, G., Ossokine, S., Pfeiffer, H. P., ... & Walker, M. (2019). The SXS Collaboration catalog of binary black hole simulations. *Classical and Quantum Gravity*, *36*(19), 195006.

[6] Caprini, C., Pujolas, O., Quelquejay-Leclere, H., Rompineve, F., & Steer, D. A. (2025). Primordial gravitational wave backgrounds from phase transitions with next generation ground-based detectors. *Classical and Quantum Gravity*, *42*(4), 045015.
[7] Chandramouli, R. S., Prokup, K., Berti, E., & Yunes, N. (2025). Systematic biases due to waveform mismodeling in parametrized post-Einsteinian tests of general relativity: The impact of neglecting spin precession and higher modes. *Physical Review D*, *111*(4), 044026.
[8] Choustikov, N. (2020). The Einstein Toolkit: A Student's Guide. *arXiv preprint arXiv:2011.13314*.
[9] Cutler, C., & Flanagan, E. E. (1994). Gravitational waves from merging compact binaries: How accurately can one extract the binary's parameters from the inspiral waveform? *Physical Review D*, *49*(6), 2658.
[10] Fishbach, M. (2024). Mystery in the "mass gap". *Science*, *383*(6680), 259-260.
[11] Gerosa, D., Kesden, M., O'Shaughnessy, R., Klein, A., Berti, E., Sperhake, U., & Trifirò, D. (2015). Precessional instability in binary black holes with aligned spins. *Physical Review Letters*, *115*(14), 141102.
[12] Goldberg, J. N., MacFarlane, A. J., Newman, E. T., Rohrlich, F., & Sudarshan, E. G. (1967). Spin-s spherical harmonics and ð. *Journal of Mathematical Physics*, *8*(11), 2155-2161.
[13] Hanna, C., Kennington, J., Niu, W., Sakon, S., Singh, D., Adhicary, S., ... & Zhang, N. (2025). Template bank for subsolar mass compact binary mergers in the fourth observing run of Advanced LIGO, Advanced Virgo, and KAGRA. *Physical Review D*, *112*(4), 044013.
[14] Kidder, L. E. (1995). Coalescing binary systems of compact objects to (post) 5/2-Newtonian order. V. Spin effects. *Physical Review D*, *52*(2), 821.
[15] Löffler, F., Faber, J., Bentivegna, E., Bode, T., Diener, P., Haas, R., ... & Laguna, P. (2012). The Einstein Toolkit: a community computational infrastructure for relativistic astrophysics. *Classical and Quantum Gravity*, *29*(11), 115001.
[16] Mac Uilliam, J., Akcay, S., & Thompson, J. E. (2024). Survey of four precessing waveform models for binary black hole systems. *Physical Review D*, *109*(8), 084077.
[17] Mastrogiovanni, S., Karathanasis, C., Gair, J., Ashton, G., Rinaldi, S., Huang, H. Y., & Dalya, G. (2024). Cosmology with gravitational waves: a review. *Annalen der Physik*, *536*(2), 2200180.
[18] Mehta, A. K., Buonanno, A., Cotesta, R., Ghosh, A., Sennett, N., & Steinhoff, J. (2023). Tests of general relativity with gravitational-wave observations using a flexible theory-independent method. *Physical Review D*, *107*(4), 044020.
[19] Newman, E., & Penrose, R. (1962). An approach to gravitational radiation by a method of spin coefficients. *Journal of Mathematical Physics*, *3*(3), 566-578.
[20] Phurailatpam, H., More, A., Narola, H., Yin, N. C., Janquart, J., Broeck, C. V. D., ... & Keitel, D. (2024). ler: LVK (LIGO-Virgo-KAGRA collaboration) event (compact-binary mergers) rate calculator and simulator. *arXiv preprint arXiv:2407.07526*.
[21] Pratten, G., García-Quirós, C., Colleoni, M., Ramos-Buades, A., Estellés, H., Mateu-Lucena, M., ... & Husa, S. (2021). Computationally efficient models for the dominant and subdominant harmonic modes of precessing binary black holes. *Physical Review D*, *103*(10), 104056.
[22] Ray, A., Hernandez, I. M., Mohite, S., Creighton, J., & Kapadia, S. (2023). Nonparametric inference of the population of compact binaries from gravitational-wave observations using binned gaussian processes. *The Astrophysical Journal*, *957*(1), 37.
[23] Sakon, S., Tsukada, L., Fong, H., Kennington, J., Niu, W., Hanna, C., ... & Wang, J. (2024). Template bank for compact binary mergers in the fourth observing run of Advanced LIGO, Advanced Virgo, and KAGRA. *Physical Review D*, *109*(4), 044066.
[24] Schmidt, S., Caudill, S., Creighton, J. D., Tsukada, L., Doke, A., Jain, M., ... & Wade, M. (2024). Searching for asymmetric and heavily precessing binary black holes in the gravitational wave data from the LIGO third observing run. *Physical review letters*, *133*(20), 201401.
[25] Shibata, M., & Nakamura, T. (1995). Evolution of three-dimensional gravitational waves: Harmonic slicing case. *Physical Review D*, *52*(10), 5428.
[26] Varma, V., Field, S. E., Scheel, M. A., Blackman, J., Gerosa, D., Stein, L. C., ... & Pfeiffer, H. P. (2019). Surrogate models for precessing binary black hole simulations with unequal masses. *Physical Review Research*, *1*(3), 033015.

[27] Yu, H., Roulet, J., Venumadhav, T., Zackay, B., & Zaldarriaga, M. (2023). Accurate and efficient waveform model for precessing binary black holes. *Physical Review D*, *108*(6), 064059.
[28] Bozzola, G. Kuibit: Analyzing and visualizing numerical relativity simulations with Python. *Journal of Open- source Software*, *6*(63), 3099 (2021). https://doi.org/10.21105/joss.03099
[29] Pfeiffer, H. P., Brown, D. A., Kidder, L. E., Lindblom, L., Lovelace, G., Scheel, M. A., & Teukolsky, S. A. (2007). Reducing orbital eccentricity in binary black hole simulations. *Physical Review D*, *76*(8), 084016. https://doi.org/10.1103/PhysRevD.76.084016